Supporting Information

New Insights Into the Effect of Residue Mutations on the Rotavirus VP1 Function Using Molecular Dynamic Simulations

Nabil Abid[1,2,*], Daniele Pietrucci[3], Marco Salemi[4] and Giovanni Chillemi[5,6,*]

[1]Laboratory of Transmissible Diseases and Biological Active Substances LR99ES27, Faculty of Pharmacy, University of Monastir, Rue Ibn Sina, 5000, Monastir, Tunisia

[2]High Institute of Biotechnology of Sidi Thabet, Department of Biotechnology, University Manouba, BP-66, 2020, Ariana-Tunis, Tunisia; nabil.abid@isbst.uma.tn

[3]Department of Biology, University of Rome Tor Vergata, Via della Ricerca Scientifica 1, 00133 Rome, Italy; daniele.pietrucci@uniroma2.it

[4]Department of Pathology, Immunology and Laboratory Medicine, University of Florida College of Medicine, Emerging Pathogens Institute, Gainesville, University of Florida, P.O. Box 100009, FL 32610-3633, USA; salemi@pathology.ufl.edu

[5]Department for Innovation in Biological, Agro-food and Forest systems, DIBAF, University of Tuscia, via S. Camillo de Lellis s.n.c., 01100 Viterbo, Italy; gchillemi@unitus.it

[6]Institute of Biomembranes, Bioenergetics and Molecular Biotechnologies, IBIOM, CNR, Via Giovanni Amendola, 122/O, 70126, Bari, Italy
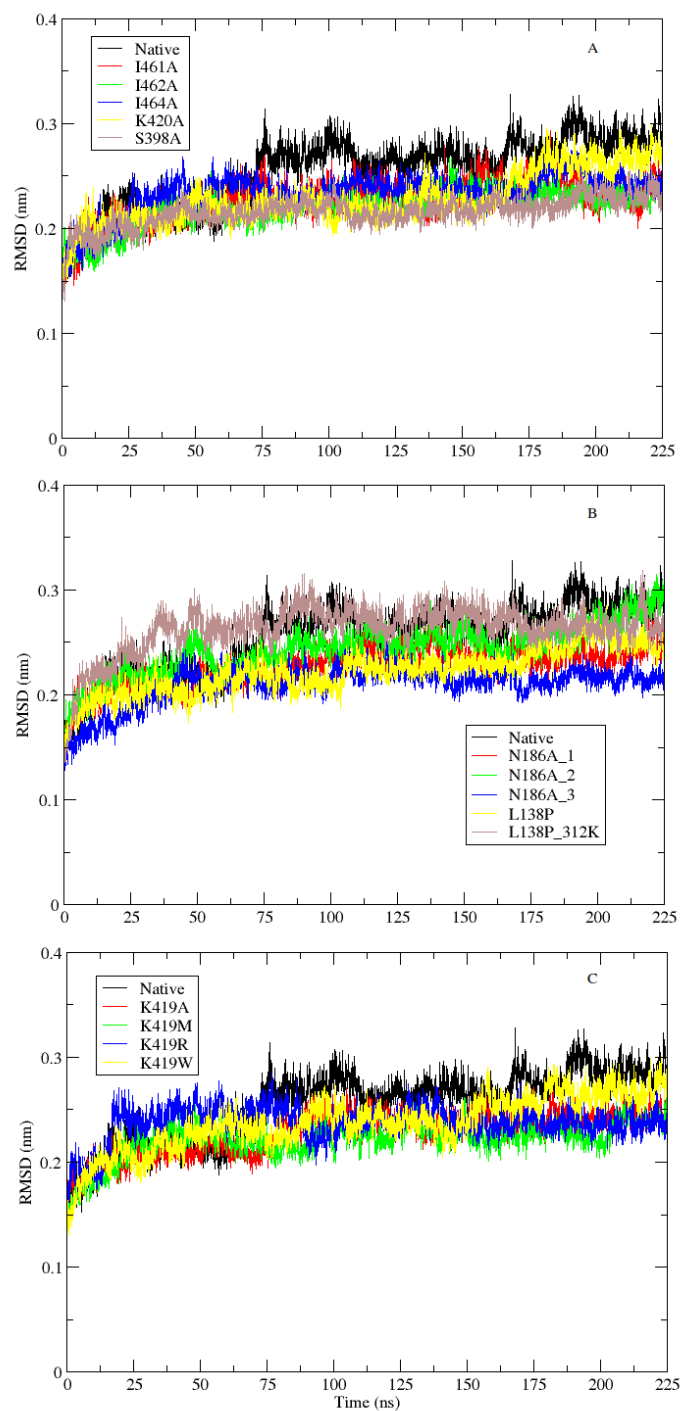
*Corresponding Author

Figure S1.

Root Mean Square Deviation (RMSD) of amino acid residues of all mutants during 225 ns simulation run. (A) RMSD of mutations of hydrophobic residues of motif F (I461A, I462A, and I464A) and finger subdomain residues (S398A and K420A); (B) RMSD of a single (N186A_1), multiple (N186A_2 and N186A_3), and temperature-sensitive (L138P) mutations; (C) RMSD of RNA entry bottleneck mutations (K419A, K419M, K419R, and K419W).
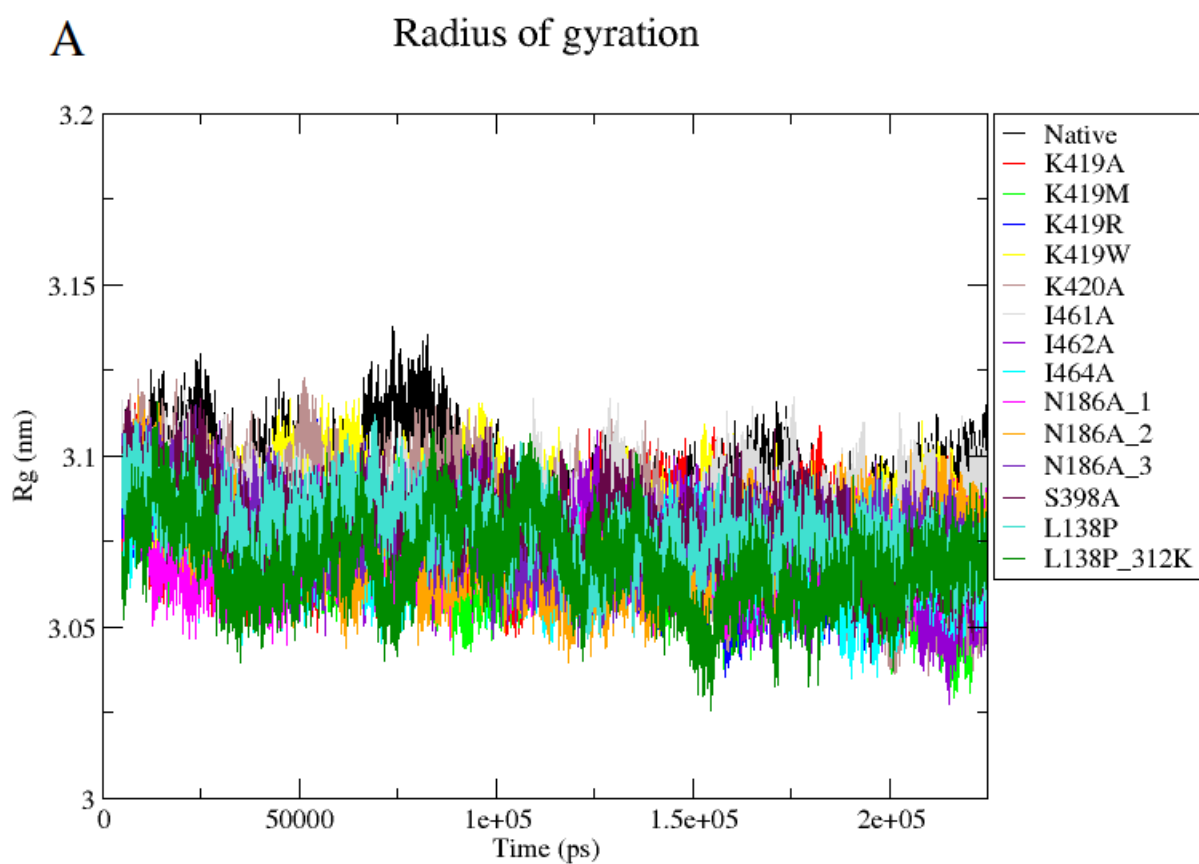
Figure S2. Radius of gyration (A) and solvent accessible surface analysis of the Native and the mutant structures. (B-F) during 225 ns simulation run. Structures are shown by different colors.
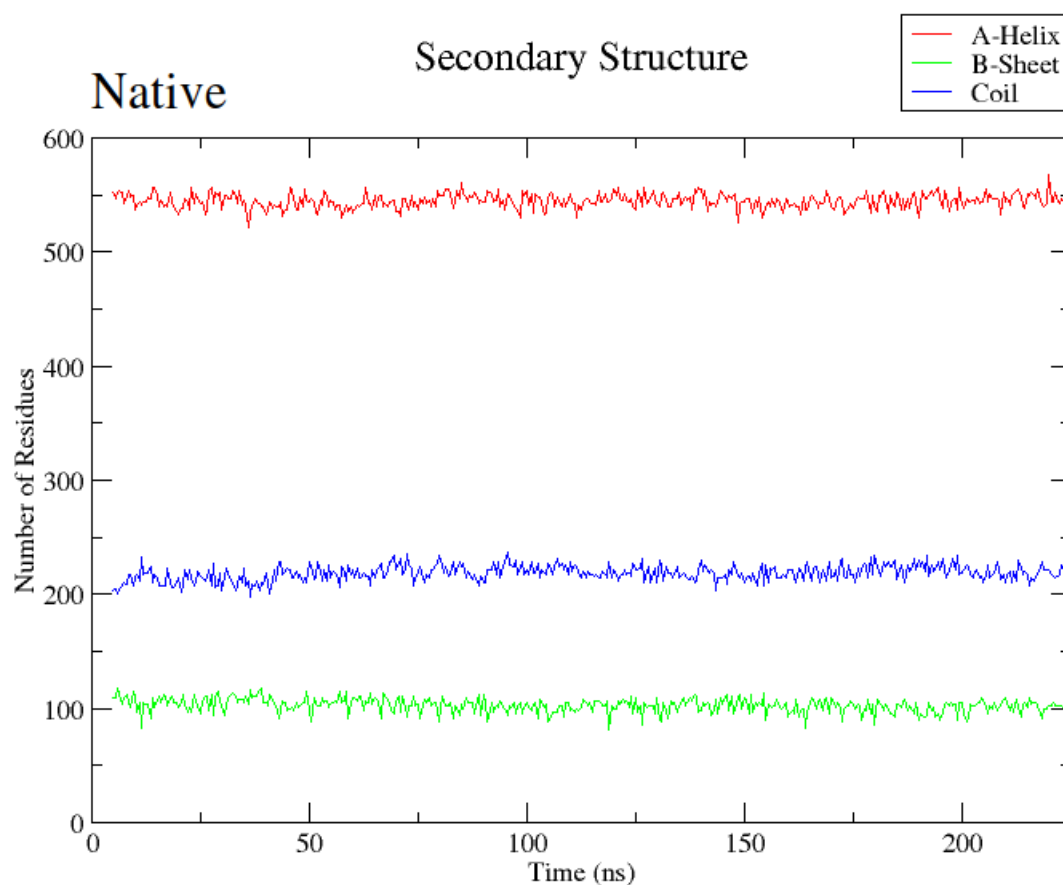
Figure S3. The secondary structure analysis of the Native and mutant structures during 225 ns simulation run. A-Helix, B-Sheet, and Coil structures are shown by different colors for all structures.
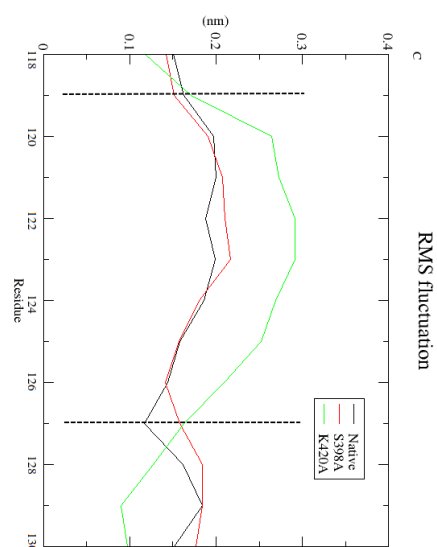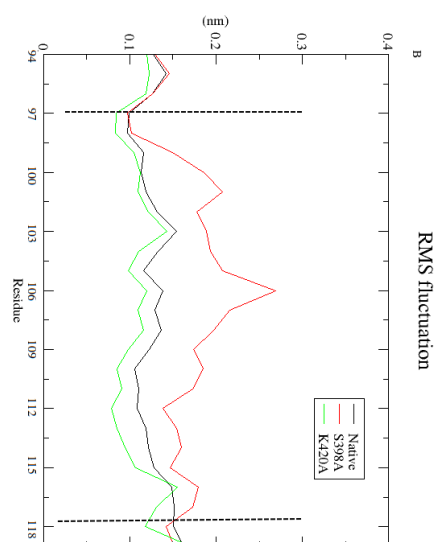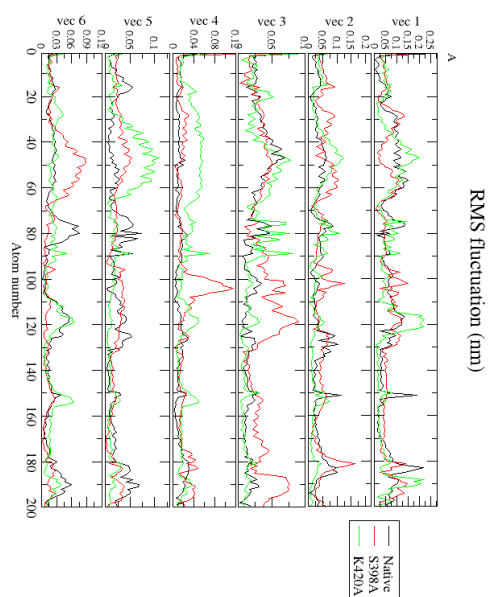
Figure S4.

Root mean square fluctuation (RMSF) values of Cα atoms of the mutants at the N-terminal region (residues 1-200) of S398A and K420A mutants calculated during 225 ns simulation run along the first six eigenvectors (A). The most pronounced fluctuations at residues 97-117 for S398A (B) and 119-127 for K420A (C).
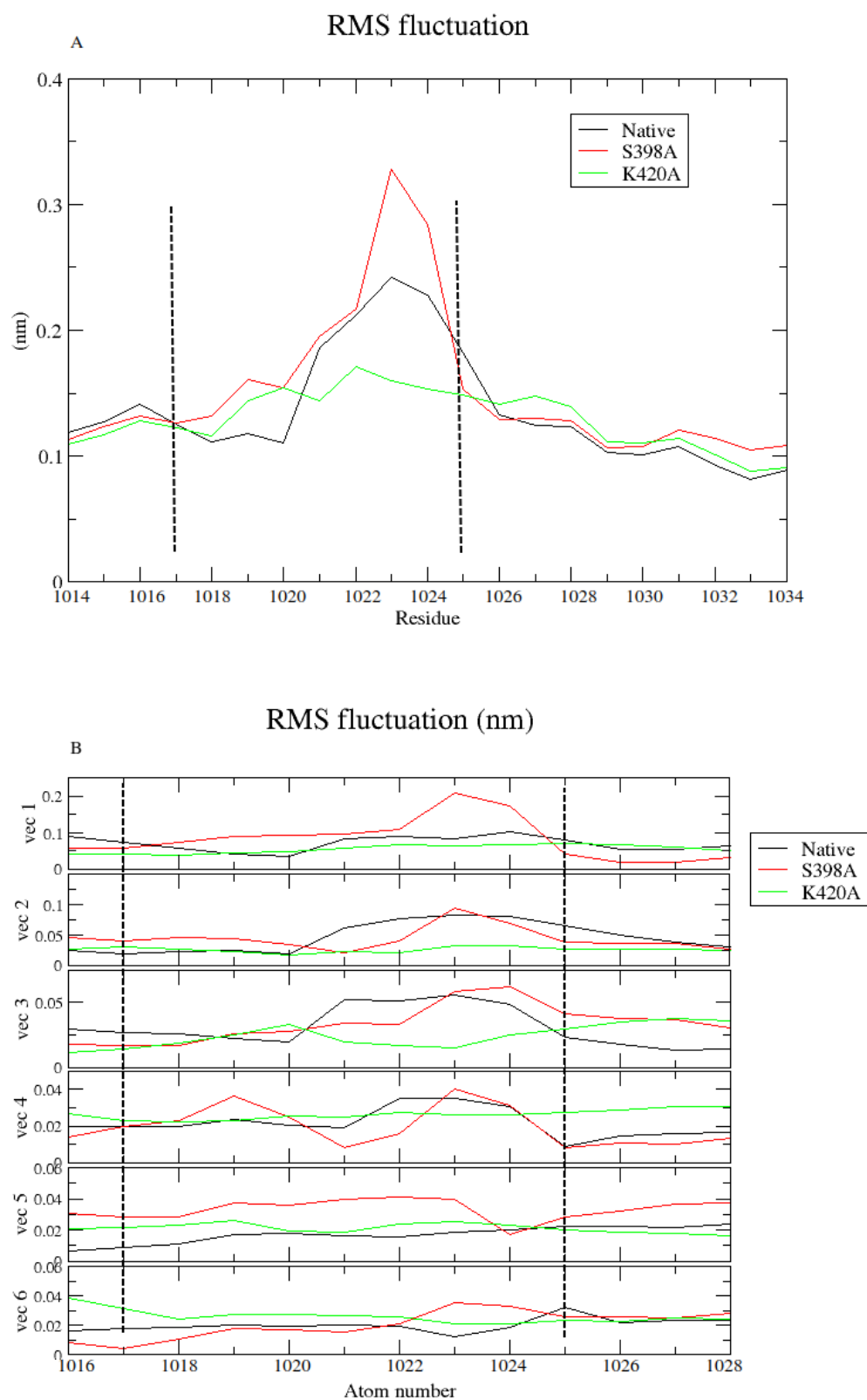
Figure S5.

Root mean square fluctuation (RMSF) values of Cα atoms of the mutants at additional region (residues 1017-1025) for S398A calculated during 225 ns simulation run (A), yet supported by the PCA analysis along the first six eigenvectors (B).
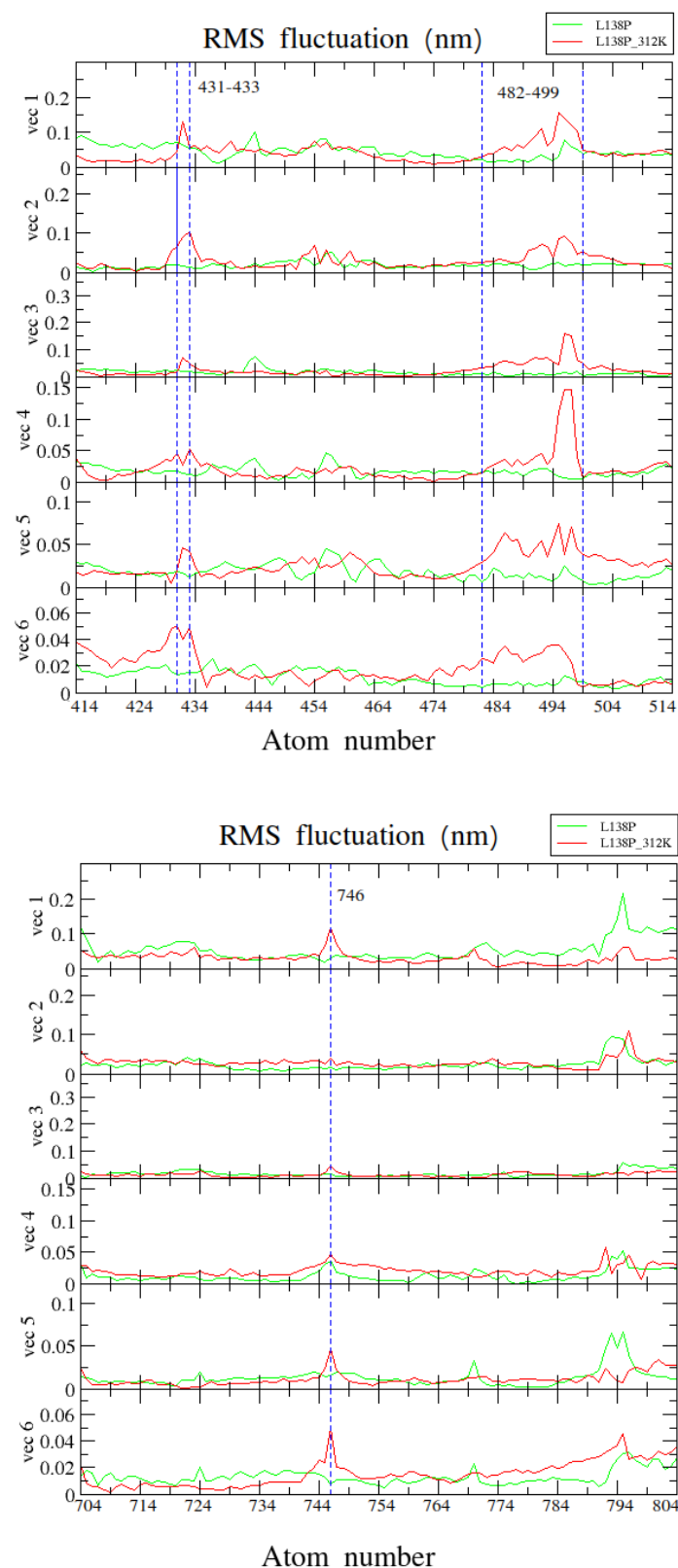
Figure S6.

Root mean square fluctuation (RMSF) values of Cα atoms of the temperature-sensitive (ts) mutants of L138P calculated during 225 ns simulation run, showing fluctuation at residue ranges 431-433, 482-499, and around residue 746, compared to L138P$_{300K}$.
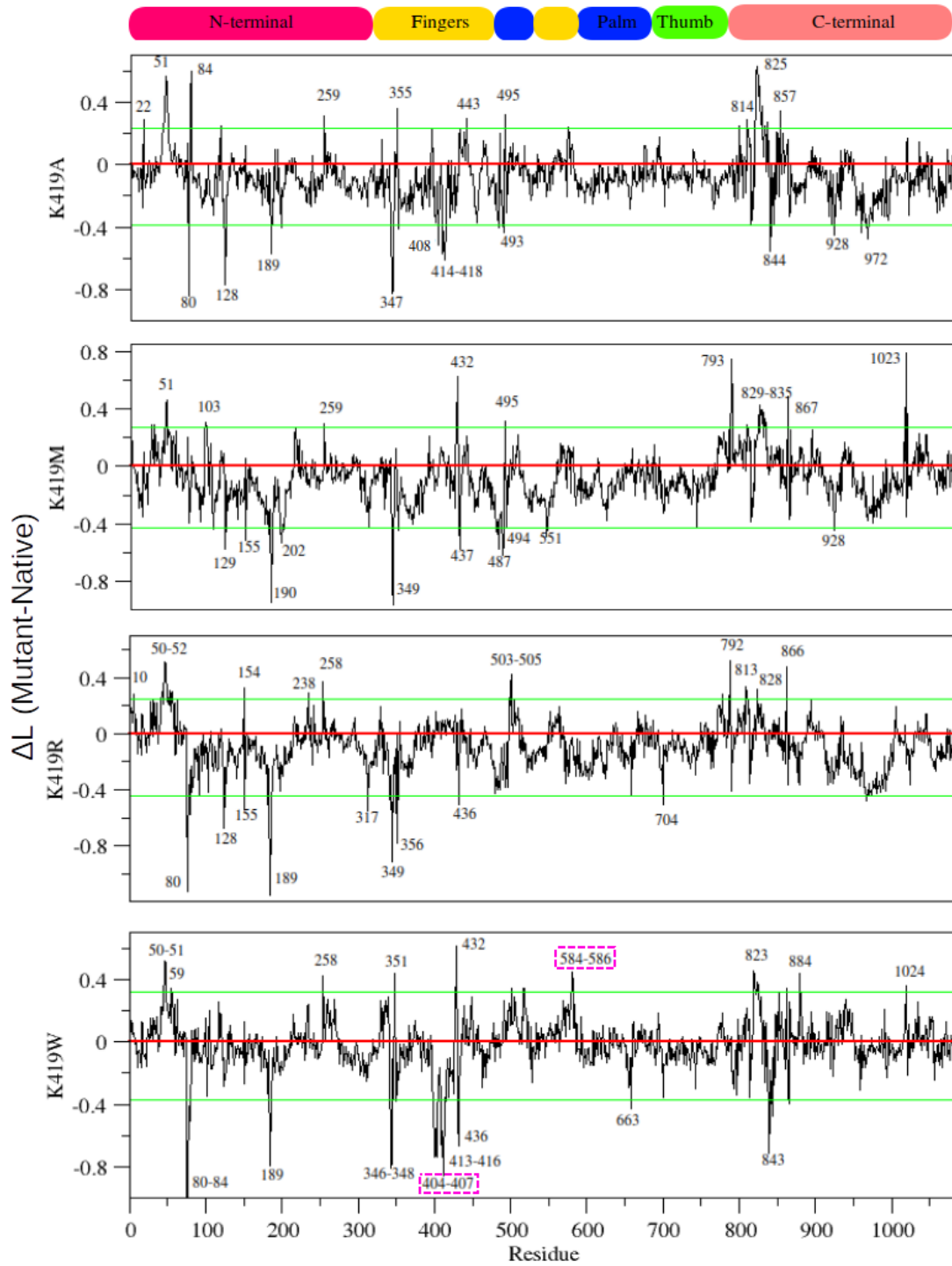
Figure S7. The measurement of reachability in VP1 protein. Change in reachability (ΔL_i) for the each protein mutant (**A-E**), compared to the Native structure. ΔL decrease indicates that residues in mutants are moving closer to each other with respect to the Native and are more accessible; whereas ΔL increase indicates that residues in mutants are moving further to each other with respect to the Native and are less accessible.
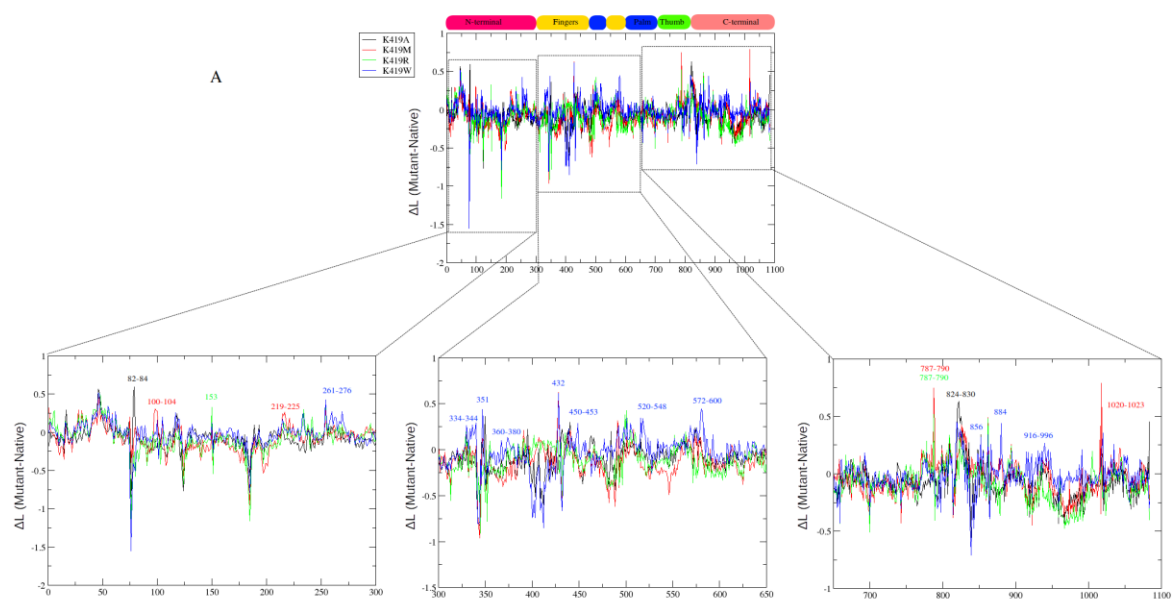
Figure S8. Multiple change in reachability (ΔL_i) analysis within protein structures. Regions recording high ΔL_i are showing by different colors according to their corresponding structures.
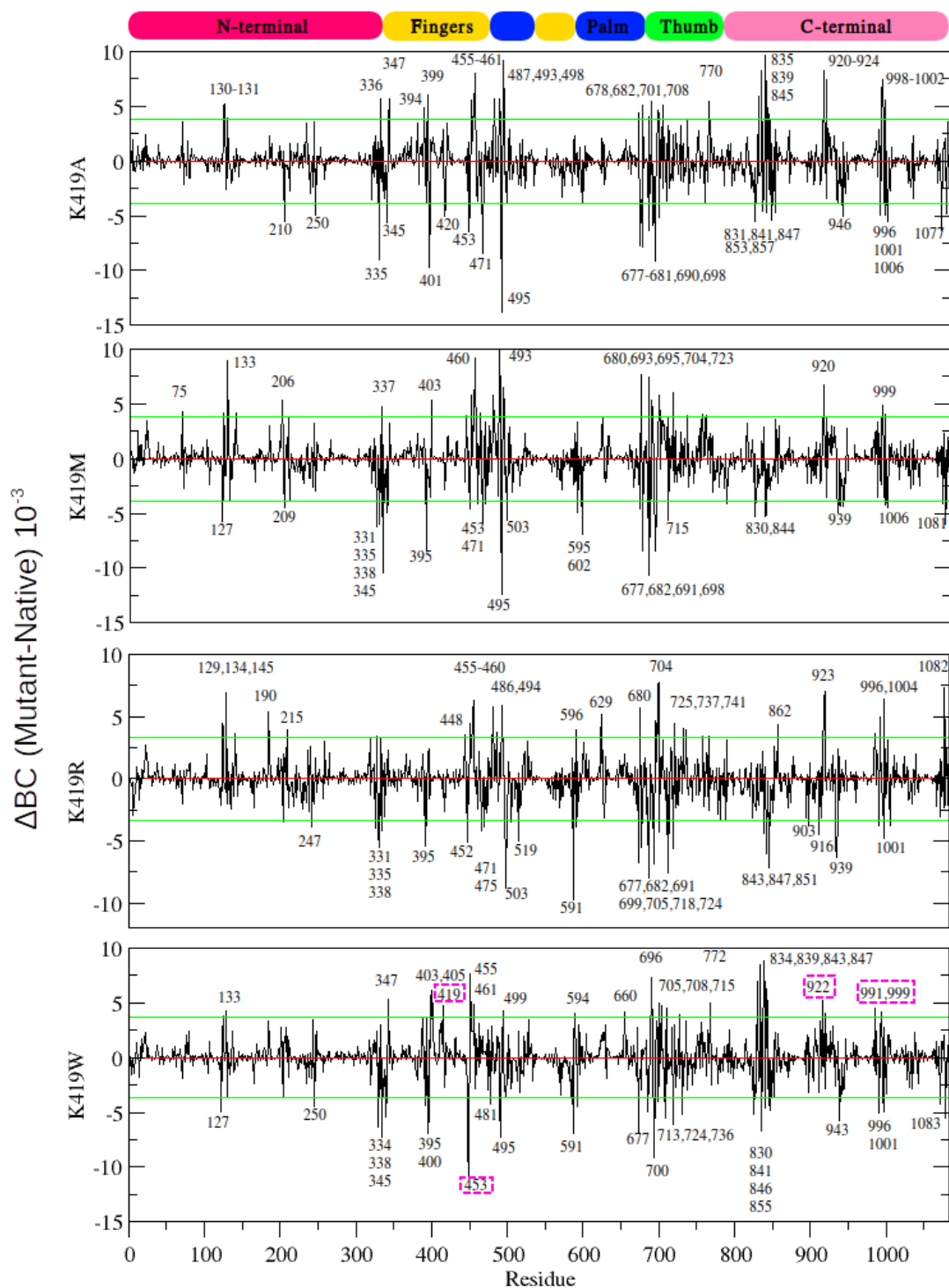
Figure S9. The measurement of betweenness centrality in VP1 protein. Change in betweenness centrality (ΔBC) profile for each protein mutant (A-E), compared to the native structure. Decrease to ΔBC indicates a decrease in residue usage within the mutant whereas an increase to ΔBC demonstrates increased residue usage.
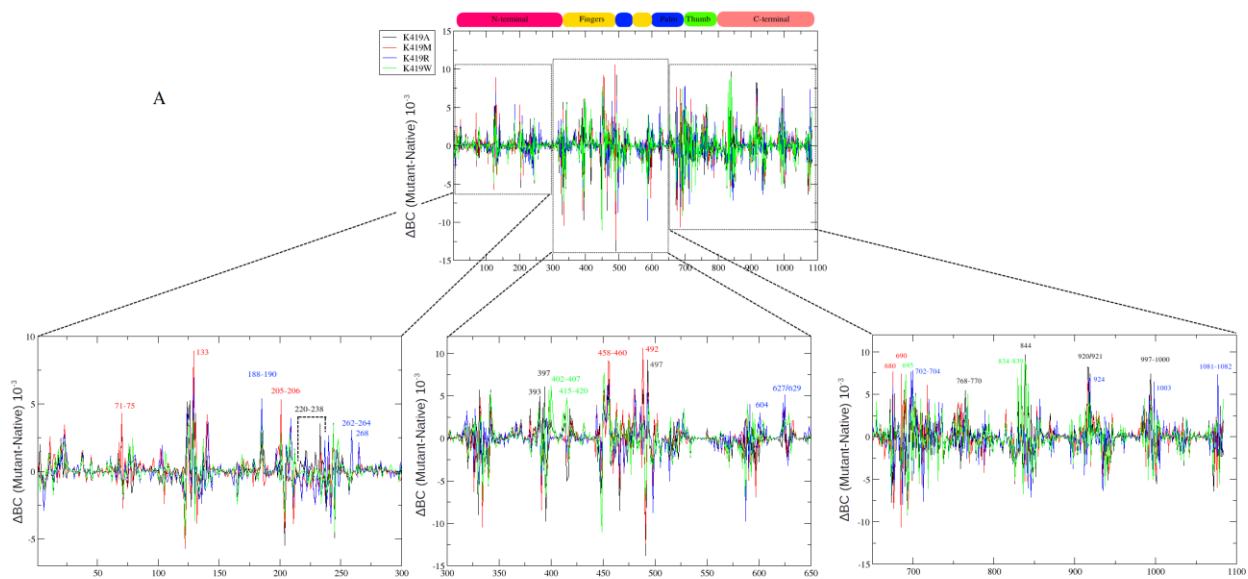
Figure S10. Change in betweenness centrality (ΔBC) profile analysis withn protein structures. Regions recording high ΔBC are shown by different colors according to their corresponding structures.
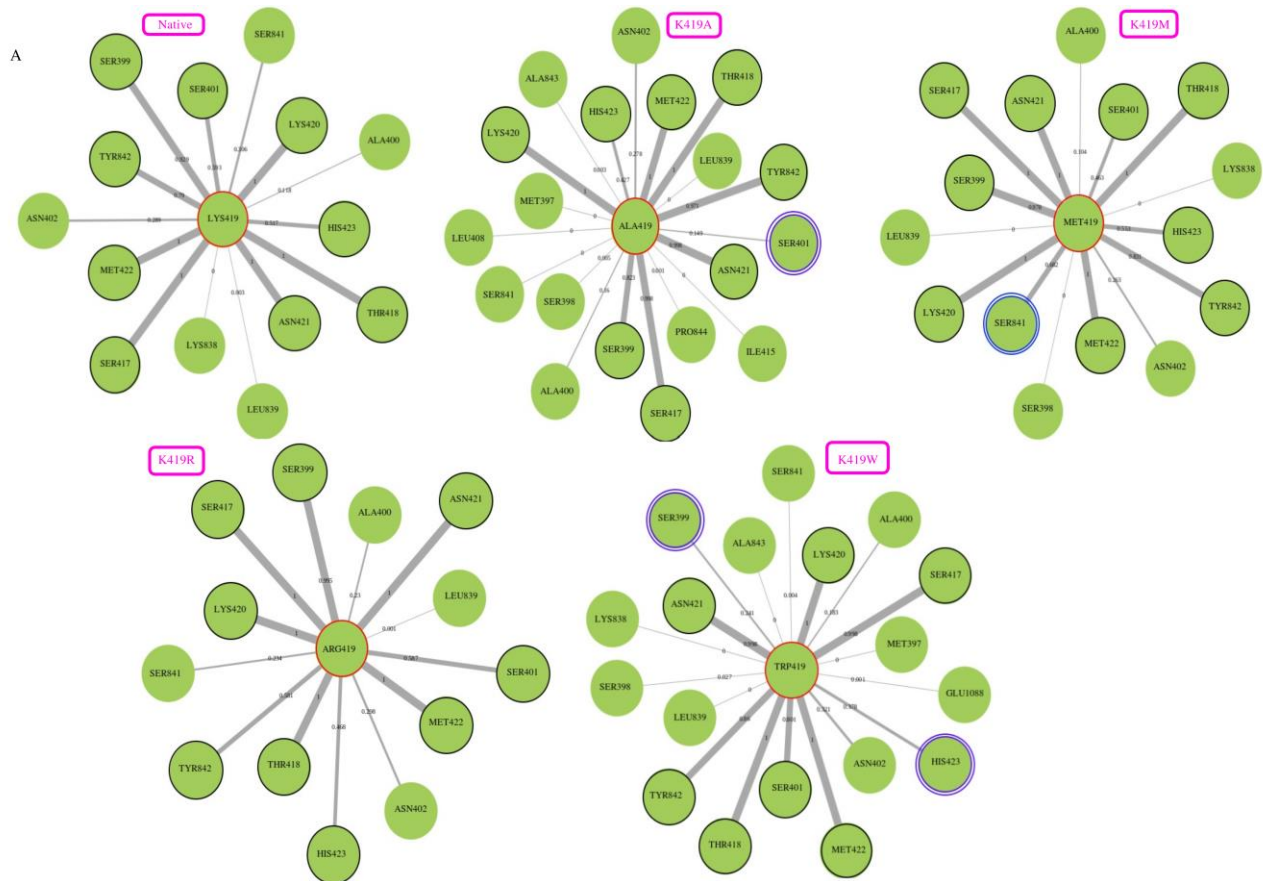
Figure S11. Residue contact maps of mutated residues, compared to the Native structure (A-G). Edges between the residue of interest and the other residues are weighted based on how often the interaction exists.
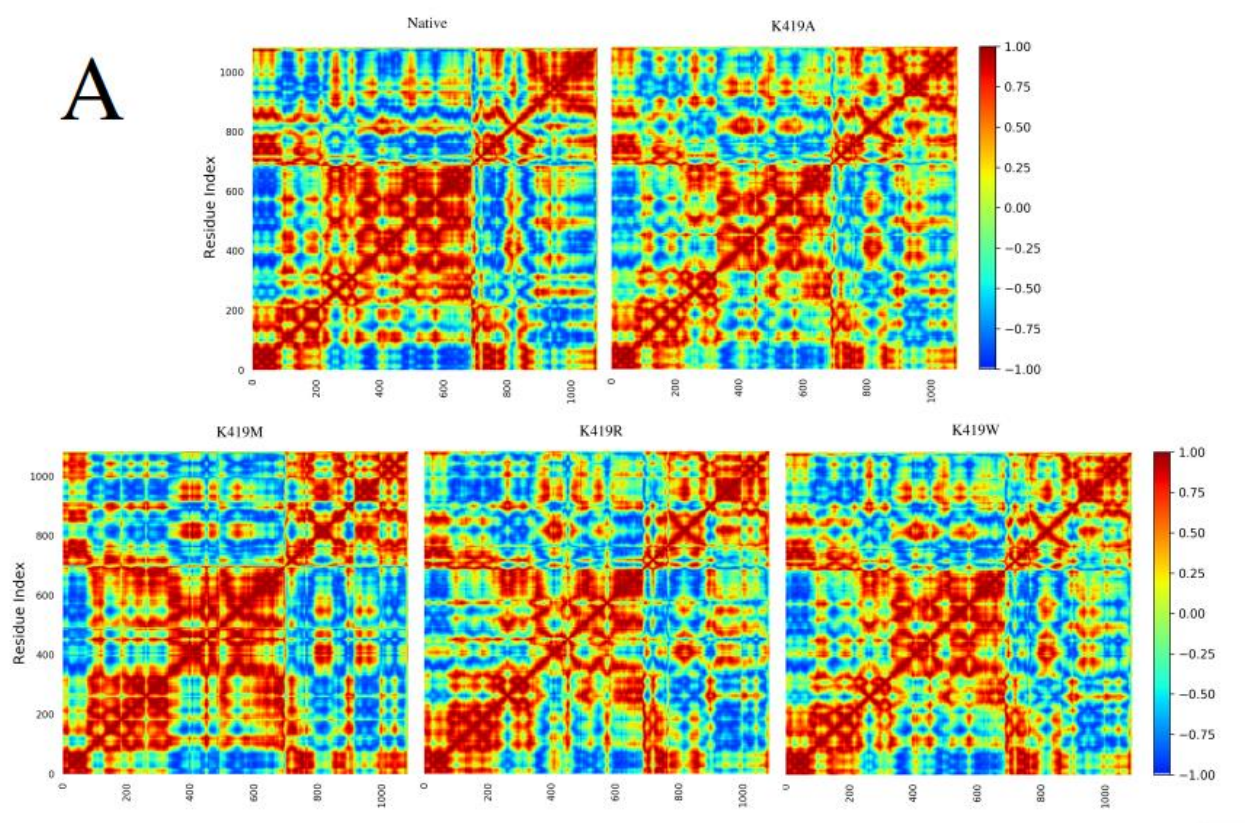
Figure S12. Dynamic cross-correlation profile of protein mutants. Matrices calculated as the difference in communication efficiency between protein residues (A-E). Warm colors (from yellow to red) indicate a relatively higher positive correlation, whereas the cold color (from cyan to blue) represents relatively highly anti-correlation.
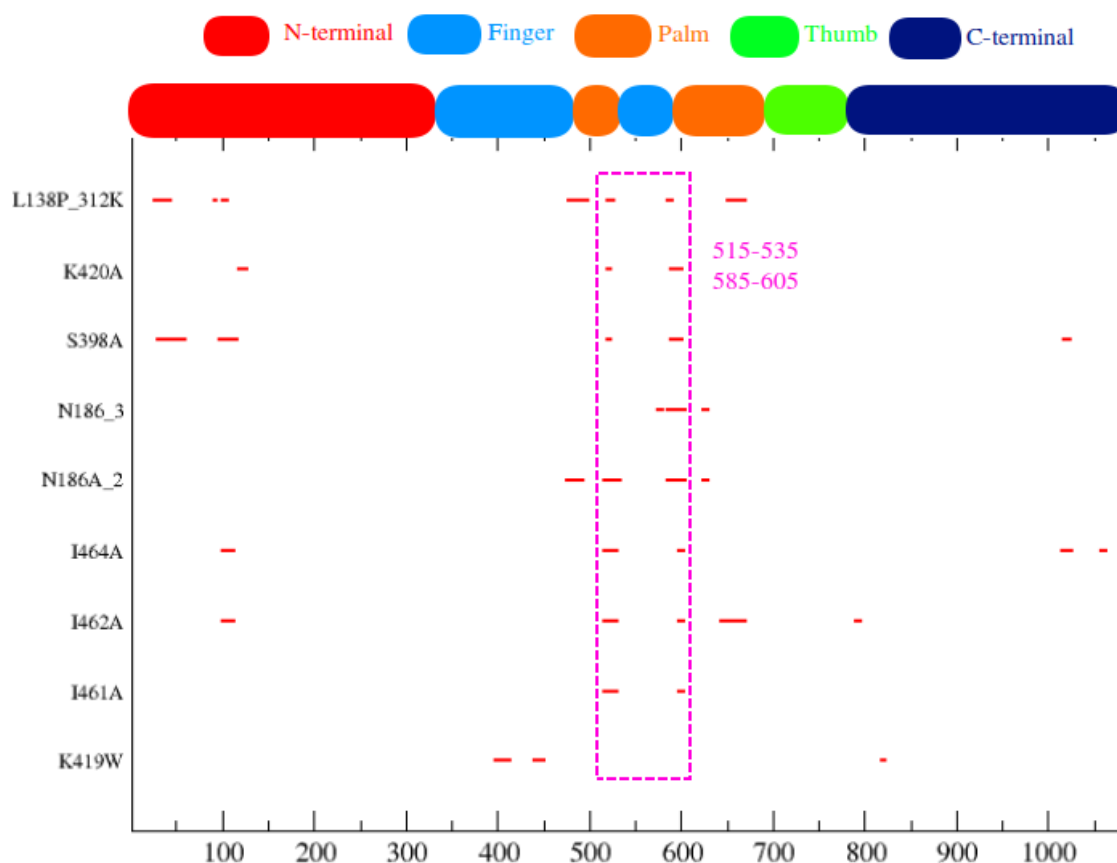
Figure S13. Difference in root mean square fluctuations (ΔRMSF) of backbone atoms in protein mutants, compared to Native structure. The fluctuations of residues were shown by horizontal lines (red). The most pronounced fluctuations (aa 515-535 and aa 585-605) were shown by magenta colored box.

Table S1. The h-bond analysis of the K419A, K419M, K419R, and K419W mutants. Time occurence of h-bond and atoms involved in interactions are shown. Differences are shown by different colors: (i) missing residues are shown by yellow; (ii) time occurrence of h-bond is shown by red; (iii) the unique residues for K419W mutant are shown by green.

| K419A							K419M							K419R							K419W						
LYS	409	N	LYS	409	H	ASP	426	OD1	94.00%	LYS	409	N	LYS	409	H	ASP	426	OD1	4.00%	LYS	409	N	LYS	409	H	ASP	426	OD1	0.70%	LYS	409	N	LYS	409	H	ASP	426	OD1	0.002%
GLY	411	N	GLY	411	H	THR	807	OG1	7.00%	GLY	411	N	GLY	411	H	THR	807	OG1	90.00%	GLY	411	N	GLY	411	H	THR	807	OG1	81.00%	GLY	411	N	GLY	411	H	THR	807	OG1	16.40%
ARG	412	NH1	ARG	412	HH11	GLY	797	O	86.00%																														
ARG	412	NH1	ARG	412	HH11	ASP	800	OD2	98.00%																					ARG	412	NH1	ARG	412	HH11	ASP	800	OD2	50.00%
ARG	412	NH2	ARG	412	HH21	GLY	737	O	95.00%																														
ARG	412	N	ARG	412	H	GLU	801	OE2	0.004%	ARG	412	N	ARG	412	H	GLU	801	OE2	91.00%	ARG	412	N	ARG	412	H	GLU	801	OE2	0.002%	ARG	412	N	ARG	412	H	GLU	801	OE2	46.00%
LYS	413	NZ	LYS	413	HZ1	GLU	848	OE2	1.50%																					LYS	413	NZ	LYS	413	HZ1	GLU	848	OE2	83.00%
LYS	413	NZ	LYS	413	HZ1	GLU	801	OE1	0.05%	LYS	413	NZ	LYS	413	HZ1	GLU	801	OE1	10.00%	LYS	413	NZ	LYS	413	HZ1	GLU	801	OE1	9.00%	LYS	413	NZ	LYS	413	HZ1	GLU	801	OE1	88.00%
SER	417	N	SER	417	H	ARG	406	O	94.00%	SER	417	N	SER	417	H	ARG	406	O	0.002%	SER	417	N	SER	417	H	ARG	406	O	5.00%	SER	417	N	SER	417	H	ARG	406	O	0.002%
LYS	420	N	LYS	420	H	SER	398	O	19.00%	LYS	420	N	LYS	420	H	SER	398	O	17.00%	LYS	420	N	LYS	420	H	SER	398	O	0.10%	LYS	420	NZ	LYS	420	HZ1	SER	398	O	0.007%
LYS	420	N	LYS	420	H	ALA	400	O	19.00%	LYS	420	N	LYS	420	H	ALA	400	O	0.005%	LYS	420	N	LYS	420	H	ALA	400	O	0.03%	LYS	420	N	LYS	420	H	ALA	400	O	0.30%
LYS	420	NZ	LYS	420	HZ1	GLU	404	OE2	27.00%																														
LYS	420	NZ	LYS	420	HZ1	ASN	402	OD1	0.002%	LYS	420	NZ	LYS	420	HZ1	ASN	402	OD1	1.00%	LYS	420	NZ	LYS	420	HZ1	ASN	402	OD1	76.00%	LYS	420	NZ	LYS	420	HZ1	ASN	402	OD1	0.015%
ASN	421	N	ASN	421	H	SER	398	O	9.00%	ASN	421	N	ASN	421	H	SER	398	O	0.004%	ASN	421	N	ASN	421	H	SER	398	O	84.00%	ASN	421	N	ASN	421	H	SER	398	O	13.00%
HIS	423	NE2	HIS	423	HE2	GLU	404	OE1	75.00%	HIS	423	NE2	HIS	423	HE2	GLU	404	OE1	0.005%	HIS	423	NE2	HIS	423	HE2	GLU	404	OE1	0.14%	HIS	423	NE2	HIS	423	HE2	GLU	404	OE2	0.009%
ASN	430	ND2	ASN	430	HD21	LYS	409	O	0.20%	ASN	430	ND2	ASN	430	HD21	LYS	409	O	4.50%	ASN	430	ND2	ASN	430	HD21	LYS	409	O	90.00%										
LYS	445	NZ	LYS	445	HZ1	ASN	402	O	89.00%	LYS	445	NZ	LYS	445	HZ1	ASN	402	O	4.50%	LYS	445	NZ	LYS	445	HZ1	ASN	402	O	10.00%	LYS	445	NZ	LYS	445	HZ1	ASN	402	O	0.60%
																														ARG	451	N	ARG	451	H	GLU	404	OE1	62.00%
																														ARG	452	NE	ARG	452	HE	GLU	404	OE1	54.00%
TYR	467	N	TYR	467	H	ASN	402	OD1	18.00%	TYR	467	N	TYR	467	H	ASN	402	OD1	0.004%	TYR	467	N	TYR	467	H	ASN	402	OD1	4.60%	TYR	467	N	TYR	467	H	ASN	402	OD1	0.002%
LYS	583	NZ	LYS	583	HZ1	GLU	404	OE1	0.005%	LYS	583	NZ	LYS	583	HZ1	GLU	404	OE1	0.002%	LYS	583	NZ	LYS	583	HZ1	GLU	404	OE1	0.15%	LYS	583	NZ	LYS	583	HZ1	GLU	404	OE1	66.00%
SER	805	OG	SER	805	HG	PHE	410	O	84.00%	SER	805	OG	SER	805	HG	PHE	410	O	30.00%	SER	805	OG	SER	805	HG	PHE	410	O	0.002%	SER	805	OG	SER	805	HG	PHE	410	O	0.07%
THR	807	OG1	THR	807	HG1	PHE	410	O	66.00%																														

Video S1. Animated visualization of the mutated residues in the VP1 protein used in the present study.

Video S2. Animated visualization of the fluctuation of the residues 400-406 of the K419W mutant, compared to K419A, K419M, and K419R using extreme structure according to eigenvector v1. Shift distance between model 1 and model 10 of the extreme structure of K419W was shown.